Introduction

The role of the racetrack surface in risk for musculoskeletal injury has been described in a number of studies. Different racetrack surfaces have different risk profiles for musculoskeletal injury, meaning that it should be possible to reduce the risk of injury to horses training or racing on a track by adapting its design or surface conditions. The first surface property studied was the surface hardness, which was positively associated with the prevalence of lameness in several studies.

Racetrack surface is still a major area of research. However, athletic injury in racehorses is complex and related to multiple factors affecting both performance and health and the relationships between surface properties and risk of injuries have not been completely established. Reducing the risk of a single cause of injury could increase the risk of other injuries. To understand the relationships between racetrack surface properties and risk of musculoskeletal injuries, it is necessary to fully understand how the tissues of the limb respond mechanically to the surface properties, including stiffness and variability.

Biomechanical models have been developed to illustrate the mechanisms allowing animals to interact with their locomotor environment. These models can be classified under three main types: conceptual models, physical models and mathematical models. Conceptual models explain a mechanism by using another one that is well understood. For example, the movement of the foot on the ground during human walking has been compared to an egg rolling from one end to the other. The purpose of this type of model is to clarify and understand simply a complex mechanism without mathematical consideration. Physical models consist of built structures. This type of model is used to demonstrate that a proposed mechanism actually works, to check the output of mathematical models, facilitate observations that would be difficult to make on a real animal, explain unexpected phenomena, and determine the consequences of changes in structures. Mathematical models represent a mechanical output with mathematical equations. These models are used for prediction, seeking an optimum and inverse optimization. This category can be subdivided into four sub-groups: the simple models, the more realistic models, the optimization models and the inverse optimization models. The simple models are the best for establishing general principles. They have been used in human, animal and insect locomotion, to explore effects of changing the properties of tendons and muscles or the number of joints, and to explain other phenomena that can be observed, such as the different shapes of bones or the feeding suction of fish. Some problems may require more realistic models, which are often used to explain more complicated movements, such as somersault or to calculate stresses in elaborately shaped bones. If these models are more realistic than simple models, the assumptions made to develop these models prevent their application in some

environments or scenarios. For instance, a model studying the ligament strains at a joint will consider the bones as rigid bodies, and although this model can be accurate for the ligaments it will never be possible to use it to study bone fracture processes.

The main challenge in musculoskeletal modelling is to build subject-specific models without intensive and time-consuming manual interventions. To represent different subjects without entirely reconfiguring the model template, it is necessary to scale a generic model. One method is to apply simple linear scaling laws to generic models, which are based on one or more cadaver specimens. The problem with this method is that the variability in musculoskeletal geometry between individuals is not considered. Several studies have focused on creating subject-specific models based on imaging or functional measurements but their clinical application on a large scale has not been demonstrated. Another scaling method is to use the medical images of the individual subject and incorporate them in the generic model.

A challenge specific to equine limb musculoskeletal modelling is to represent the stay apparatus. Indeed, the interactions between the digital flexor muscles and their accessory ligaments have not been studied when a detailed mathematical model of these interactions is necessary to determine accurately the forces generated by the muscles, tendons and ligaments and for a thorough analysis of the work done by each of these structures.

It would be useful to understand how tendons and ligaments transmitting force in the limb respond to different surface properties. It should be possible to determine the surface properties reducing the risk of a specific musculoskeletal injury while checking they are not increasing the risk of musculoskeletal injury in another element of the limb. The best way to answer these questions is to use a musculoskeletal model. These have been developed to illustrate and understand how animals interact with the environment but allow also to study the loads in muscles, tendons and ligaments, which is important to understand the origin of musculoskeletal injuries. To date, equine musculoskeletal models have focused mainly on the distal limb. The objective of this study was to create a 3D musculoskeletal model of the entire horse forelimb and answer the following questions:

1 - When a limb hits a surface that is unexpectedly harder or softer, when does the limb respond, and how?
2 - Can we observe, with the model, differences in tendon and ligament strains according to the gait data resulting from the perturbations?

Experiment 1: Development of the model and preliminary testing

We developed our limb model using a musculoskeletal modelling package called AnyBody™ (see www.anybodytech.com).

Bones: A Thoroughbred forelimb was dissected free of its muscles and then CT images obtained with a Phillips Brilliance 16-slice helical scanner (Phillips Healthcare, The Netherlands) with a voxel size 0.8 mm x 0.8 mm x 0.8 mm, a 1 mm slice thickness and a 0.5 mm overlay. CT images were then processed using YaDiV (Welfenlab, Leibniz Universität Hannover, Germany). A 3D image was created for each single bone, and the centre of mass and principal moments of inertia were computed using Solidworks.

Muscles: The limb was meticulously dissected, mapping out detailed origins and insertion points for each muscle and ligament. Morphometric variables (muscle mass, muscle volume, pennation angle, muscle fibre length, tendon slack length…) were recorded for each muscle and samples of each muscle were dissected out for histomorphometry, to record sarcomere lengths.

AnyBody allows the use of three different muscle models: the simple model, the 2-element Hill model and the 3-element Hill model. All models require origin and insertion points, and either points or wrapped surfaces can be used to define the muscle/tendon path. However, only one origin and insertion site can be defined for a muscle, which means that a muscle with more than one head of origin or insertion site needs to be modelled as different muscles.

The simple model represents only the contractile element of the muscle. This makes it easier to use as it needs only one parameter, the maximal isometric force. However, it does not include the passive elastic properties of the muscle or tendon.

The 2-element Hill model represents a contractile element for the muscle fibers and a serial elastic element for the tendon. In this model, the force-length and the force velocity relationships of the contractile element as well as the force-length relationship of the serial element are linear. The 3-element Hill model includes a contractile element for the active muscle fibers, a non-linear serial elastic element for the tendon and a non-linear parallel elastic element for the passive part of the muscle fibers. If these models are more realistic, by representing the action of the muscle and the passive action of the series elastic elements (for the 3-element model), they also need more muscle-tendon parameters, which can be complicated to quantify, such as the maximum contraction velocity.

Ligaments: The ligaments are modelled by a polynomial force-length equation. The parameters required are the slack length and the values of the strain and the corresponding force. As for the muscles, their path is defined by origin and insertion sites and "via points" or wrapped surfaces can be added. A ligament with more than one origin or insertion site needs to be modelled by several ligaments. The ligament properties and stress-strain relationships were determined in a parallel project being run in our lab by a Master's student.

Model: The models developed with AnyBody can be run with two programmes: kinematics and inverse dynamics. The kinematics programme only calculates the position of the different limb segments based on the input gait data. This data can be obtained via either marker positions or by angular position of the joints. The inverse dynamics programme uses data from the kinematics programme and computes the forces within the ligaments and muscles. The loads are shared between the different muscles by optimisation.

To create the model with AnyBody, a template was used. This template was created based on AnyBody Managed Model Repository files. From this template, a segment was created for each single bone, using the 3D images from CT and their mechanical properties. The initial position of the bone was determined by the distance between the center of mass of the bone and the points of reference introduced in the CT scan images. The initial position of the segment is defined by the initial translation (r0) and rotation of the segment compared to the global reference frame. The values of r0 and of the initial rotation of the segments were then modified manually to configure the bone's location in the standing horse.

Using Solidworks, the local coordinates of points representing the muscle and ligament origin and insertion sites on the segmental bony surfaces were located; the local coordinates of the points at the centre of the joint bony surfaces were computed, these points that will later be called "reference nodes; these coordinates were used to create the points on the segment in AnyBody. The muscles were modelled as 3-element Hill muscles if their pennation angle was greater than 20deg, and as 2-element muscles if less than 20deg.

The final model was composed of three sequential parts: Scaling, Calibration, DynamicTrial.

The Scaling part can only be run with the kinematic programme. It positions the segments by the distances and rotation of the nodes on the joint bony surfaces and scales the segments and joint geometries. It then computes the local coordinates on the segment that does not contain the centre of rotation of the joints (on the scapula for the shoulder, on the antebrachium for the elbow, on the carpo-metacarpal segment for the carpal joint, on the pastern for the fetlock and on the hoof for the

coffin). It also computes the joint flexion, abduction and rotation of the joints, and the lengths of the muscle-tendon units and ligaments, so all the data for the scaled model are saved.

The Calibration part can likewise only be run with the kinematic programme. It positions the segments by using the calibration marker locations while constraining all the joint translations to be null and all the joint abduction and rotation, as well as the flexion of the shoulder and coffin, with the data computed in the scaling part. The only movement allowed in this part is thus the flexion/extension of the elbow, carpal and fetlock. It then computes the local coordinates of the kinematic markers.

The DynamicTrial part can be run with either the kinematics or the inverse dynamics. However, to compute the forces within the muscles, it is necessary to run the inverse dynamics. Only the flexion and extension of the limb joint is allowed, the translations of the joint are constrained to be null and the joint axial rotations and abductions are constrained to be those saved in the scaling part. For each step, the model positions the segments by using the kinematic markers and respecting the joint constraints. For the whole motion, it computes the individual joint angles, muscle forces, ligament and tendon strains, the predicted ground reaction force, the velocity of the horse and the compression of the limb.

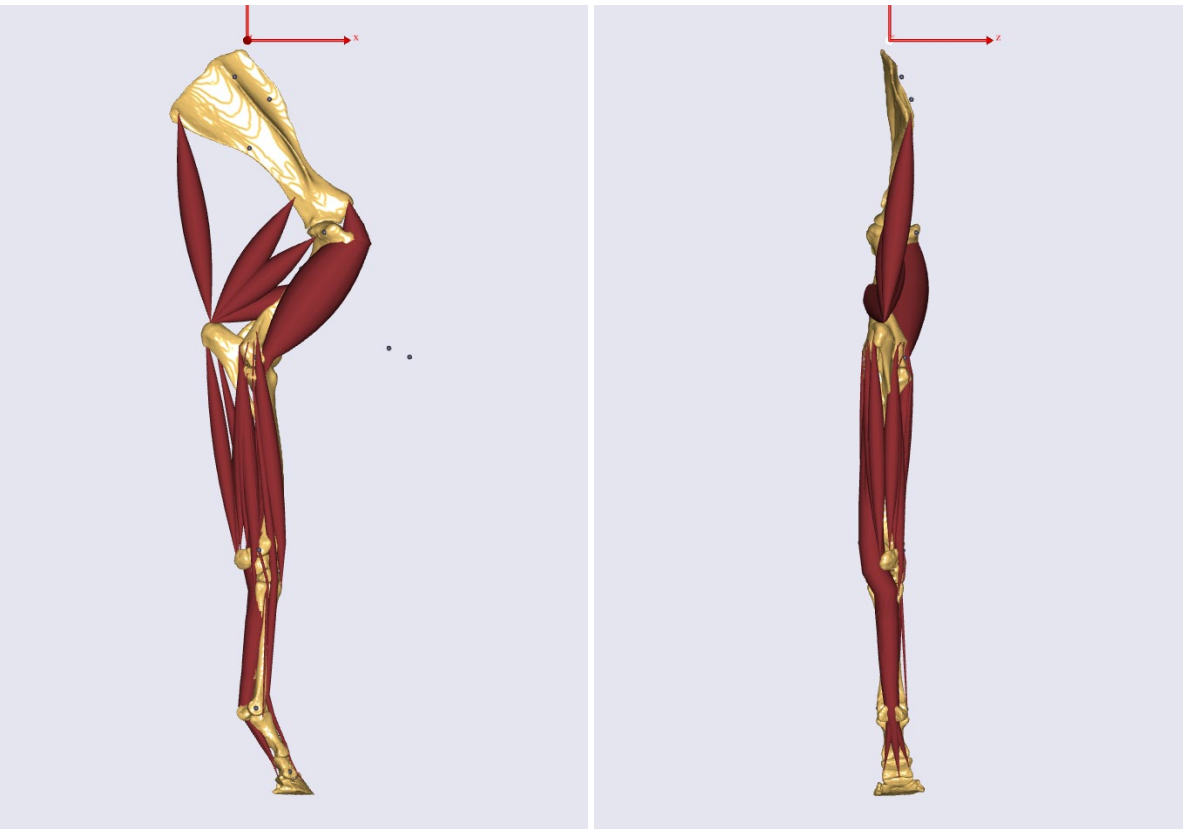

Gait trials

Concurrent with development of the AnyBody model, gait data were collected from 4 Thoroughbreds to use for testing of the performance of the model. Data were collected in an indoor riding arena (60m x 30m) at a commercial equestrian centre. The surface of the indoor school consisted of a sand mixture, approximately 6 cm deep. The volume of interest was defined by the beginning of the stance phase to the end of the following swing phase, with a height corresponding to the highest point of the withers of the horse. Kinematic data were captured via six Qualisys cameras placed on one side of the runway, and oriented so at least three cameras would have all the limb markers in their field of view during a whole stride (at trot and canter). The whole 3D volume of the runway was calibrated with the use of a reference frame and a calibration wand.

Kinematic data were captured using 18 spherical passive markers taped to the skin of the forelimb. Each limb segment (scapula, brachium, antebrachium, carpus/metacarpus, pastern and hoof) was defined by a group of three markers. Eight spherical calibration markers were taped on the centre of rotation of each joint: one on the lateral side of each joint (shoulder, elbow, carpal, fetlock and coffin) and one on the medial side of the distal joints (carpal, fetlock and coffin).

The horse was then brought into the calibrated volume to collect the marker positions while standing, to subsequently use in the model to place the 18 markers at the correct position. Once these data were collected, the 8 calibration markers on the joint rotation centres were removed, leaving only the segmental markers. The horse was then ridden in front of the cameras for multiple trials at trot and canter and the data saved. The runway was raked between trials to ensure the ground surface was not compacted by the previous pass. The gait data were then processed with Qualisys Track Manager and converted to c3d format for use in the AnyBody model.

Results

Representative outputs from the model, using the data from one horse at trot, are illustrated below. These were compared with data from the literature, and in general, good agreement was observed notwithstanding that our data was collected from ridden Thoroughbreds on a sand surface. Most gait studies are run with horses on treadmills or led in hand without a rider. The preliminary model was presented at the 2017 Annual Meeting of the Australia and New Zealand Association of Clinical Anatomists (Auckland, NZ) and the first model outputs at the 2018 International Conference on Equine Exercise Physiology (Lorne, Australia).

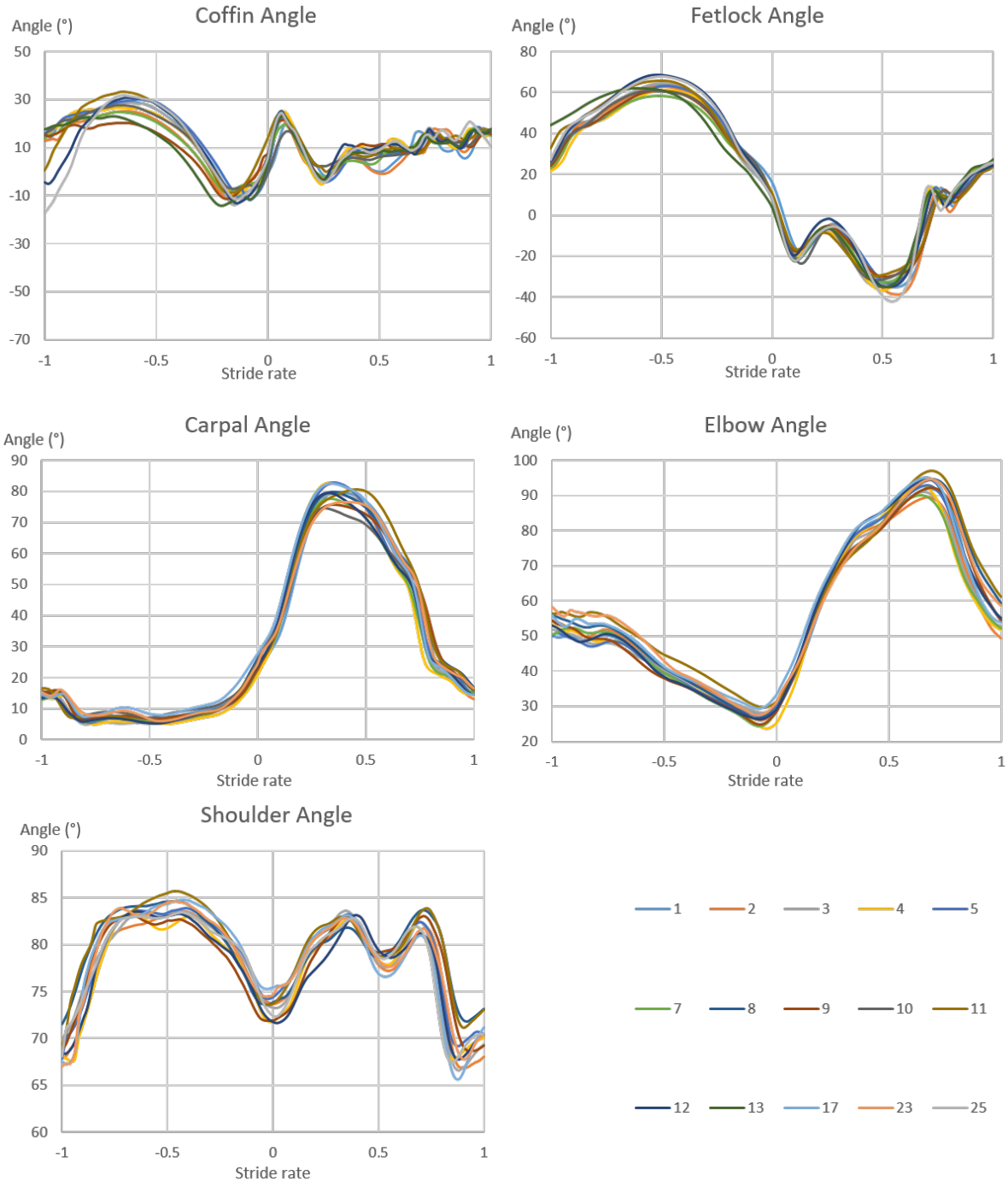

Joint angles computed from one horse at trot

Conclusion

The joint angles computed by the AnyBody model were in reasonable agreement with data reported in the literature. The small discrepancies observed would have had different origins, including the breed of the horses, their trotting and cantering velocities, whether they were running overground or on a treadmill, and whether they were ridden or not. Some studies used skin mounted markers, and some used bone mounted marker triads. There were no studies found in the literature that duplicated the conditions of our data collection methods.

We analysed the effects of trotting and cantering velocity in our trials. With increasing trotting velocity, coffin joint flexion and extension during the stance phase increased. This energy created may be stored in the tendons of the deep digital flexor and the extensor branches in the form of strain energy. The hyperextension of the fetlock also increased, and the surplus of energy created by this movement may be stored in the tendons of the deep digital flexor, the accessory ligament and tendon of the superficial digital flexor, the suspensory ligament and the straight and oblique sesamoidean ligaments in form of strain energy. The hyperextension of the carpal joint also increased. The related energy may be stored in the lacertus fibrosus, accessory ligament of the superficial digital flexor and tendons of the deep and superficial digital flexors. The energy stored in these ligaments and tendons was then released during the swing phase by increasing the last fetlock flexion of the swing and the carpal flexion. However, the intensity of increase of the flexions during the swing phase seemed much greater than the intensity of increase of the flexion/extension during stance. It might be related to the viscoelastic properties of the ligaments. Indeed, in addition to greater maximal strains observed in the tissues named earlier, the maximal strain rate of the suspensory ligaments, the accessory ligament of the superficial digital flexor, the oblique and straight sesamoidean ligaments during both stance and swing phases and the maximal strain rate of the extensor branches and tendon of the superficial digital flexor during the swing phase increased. Greater strain rate in viscoelastic material means the forces are greater. These additional forces could be the origin of the amplification (during the swing phase) of the variation generated by an increased trotting velocity during the stance phase.

Cantering velocity only affected the leading limb's shoulder extension at the stance-swing phase transition. However, with increasing cantering velocity, the maximal strain of the superficial digital flexor increased. It may be caused by the velocity delaying the first flexion peak of the fetlock of the swing phase. But the energy stored then did not lead to other variations in joint excursions to be released. It can be supposed that the energy is diffused by different joints (the superficial digital flexor tendon crosses the fetlock, carpal and elbow joints) resulting in no significant differences.

Cantering velocity had more effects on the trailing forelimb, due to its role of stopping the downward movement of the cranial trunk, head and neck of the horse. An unexpected observation was the decreased coffin flexion during stance with increasing velocity. It could have been to store more energy within the tendons of the deep digital flexor but no significant effect on their maximal strain was observed. With increasing cantering velocity, the carpal flexion at impact and the shoulder flexion of the stance phase increased. Those changes did not cause changes in ligament and tendon strains. That could mean that there is another energy storage or that the tissues storing the energy vary, independently of the horse velocity, resulting in no significant effect. The energy, supposed to be stored during the stance phase, is then released during the swing phase through a larger amplitude of movement of the coffin joint and an increased elbow flexion. As observed at trot, the maximal strain rates of the soft tissues may be involved. The maximal strain rates of the accessory ligament and tendons of the deep digital flexor increased during both stance and swing phases, the maximal strain rate of the superficial digital flexor tendon increased during the stance phase and the maximal strain rate of the extensor branches and the accessory ligament of the superficial digital extensor increased during the swing phase. The forces generated may explain the changes in joint excursion during the swing phase.

One of the limitations of musculoskeletal models are the accuracy of the model inputs. The reliability of force predictions is affected by the accuracy of the gait data collected and of the musculoskeletal geometry. Indeed, noise present in the gait data will create noise in all the data computed (joint angles, forces). The musculoskeletal geometry is said to be one of the most sensitive parameters. It is represented by muscle moment arms, and its estimation depends on the identification of the muscle-tendon lines-of-action, which is defined by their origin and insertion sites as well as by the points added to fix their positions. Another limitation to the preliminary model is the nature of the muscle models. To model the effects of the muscles more realistically, further input data will need to be provided, including muscle shortening velocity, percentage of fast and slow twitch muscle fibres and their relative contributions to tension, as well as the contributions of serial elastic components in the muscles. This will be the next step in the further development of the model.

Experiment 2: The effects of hard and soft perturbations on joint kinematics and tendon and ligament strains

The objective of this study was to determine if the equine forelimb can respond to changes in the ground surface within a perturbed stance phase or during the following stance phase. We collected data from the stance phase when the limb hit the ground in the perturbation area, the swing phase and the following stance phase in the same trial. Five privately owned Thoroughbred horses were recruited, with their normal riders, for the study. To test the model with a variety of different sized horses, they ranged in body mass from 450kg to 600kg. Each horse was observed at trot and deemed to be sound.

Data were collected in an indoor riding arena (60m x 30m) at a commercial equestrian centre. The surface of the indoor school consisted of sand, approximately 6 cm deep. In the middle of the length of the arena, a "perturbation pit" (18 cm x 120cm x 120cm) was excavated. There were three surface conditions tested:

1. Baseline: Wood stringers (12cm x 12cm x 120cm) were placed side by side in the perturbation pit and the rest of the depth was achieved by covering the wood stringers with 6cm of sand such that the surface was flush with the rest of the runway. This condition mimicked the rest of the riding surface.

2. Hard perturbation: The wood stringers were removed, and 5cm of sand was added to the pit. The wood stringers were then positioned side by side in the pit and covered with approximately 1cm of sand.

3. Soft perturbation: The wood stringers were placed in the pit and covered with a 5cm foam slab. This was then covered with approximately 1cm of sand such that the surface was again flush with the rest of the runway.

In all cases, the perturbation pit was covered with sand, and was invisible to the horse on approach. The cameras were positioned on the right side of the runway to cover the runway volume including the perturbation pit, through the stance phase of the following stride. The data were collected from five horses on five different days. To reduce the time taken to change the perturbation pit between conditions, each horse began with the hard perturbation, followed by the baseline and finished with the soft perturbation. Each horse began by performing as many trotting trials as were necessary to have the right forelimb land cleanly in the middle of the perturbation area a minimum of five times. Then, the procedure was repeated at right lead canter, such that the right forelimb landed cleanly in the perturbation area for a minimum of five trials.

The model used in this study is the one that was developed in Chapter 2. It is composed of 6 segments: scapula; brachium; antebrachium; all carpal bones, metacarpus and proximal sesamoid bones; pastern; distal phalanx and navicular bone. The inertial properties of the segments used are those reported in the literature.

The model includes 9 muscles (lateral and common digital extensors, extensor carpi radialis and obliquus, ulnaris lateralis, flexor carpi radialis and ulnaris, superficial and deep digital flexors) and 17 ligaments (accessory ligaments of the deep and superficial digital flexors, suspensory ligament, medial and lateral oblique sesamoidean ligaments, straight sesamoidean ligament, extensor branches, lacertus fibrosus, and all the collateral ligaments). The muscles and ligaments that have more than one origin and one insertion site are modelled as several separate units to represent their different lines of action. The muscles were modelled by a 2-element Hill model if their pennation angle was less than 20° and by a 3-element Hill model if their pennation angle was greater than 20°.

The AnyBody™ model was composed of 3 different parts. The Scaling part scales the segments and positions them in the standing position. The Calibration part positions the segments by using the calibration marker locations while constraining all the joint translations and all the joint abduction and axial rotation to be null. The DynamicTrial part computes the movement of the limb based on the kinematic marker positions. Joint angles, muscle forces, ligament forces, speed of the horse and compression of the limb are also computed and saved in files.

Statistical analysis was performed using R (CRAN, https://cran.r-project.org/, version 3.6.0). Analysis of variance (ANOVA) was used to test the effects of the soft (SoftPert) and hard (HardPert) perturbations on the values of interest of the curves. Baseline condition was level one of the Condition factor, which means that the values associated with the baseline were used as reference to calculate the effects of the other conditions (HardPert and SoftPert). To account for variation in joint motion between horses, 'Horse' was included as a random variable. Horse velocity and the number of the trial were included as independent factors in the statistical model and removed in turn to determine the best model. The evaluation of the statistical model was based on the AIC (Akaike information criterion). The AIC was computed for each statistical model tested and the best model corresponded to the smallest value of AIC. For this study, the best statistical model determined included the perturbation and the velocity as independent factors but not the trial number. The interactions of horse velocity and perturbation were not included because the aim was to study the effects of the perturbations. Finally, the statistical model chosen was evaluating the effects of the perturbations (hard and soft) compared to the baseline with the effect of velocity accounted for.

The values of interest are the amplitude ("y") and timing ("x") of each discrete identified peak of the joint excursions and the maximal strains and strain rates of the ligaments and tendons. Each of these was tested separately as the dependent variable in the ANOVA. Trot and right lead canter were tested separately.

Results: Representative data are presented for the coffin joint. The Table on the following page relates to the x and y positions in the following graph.

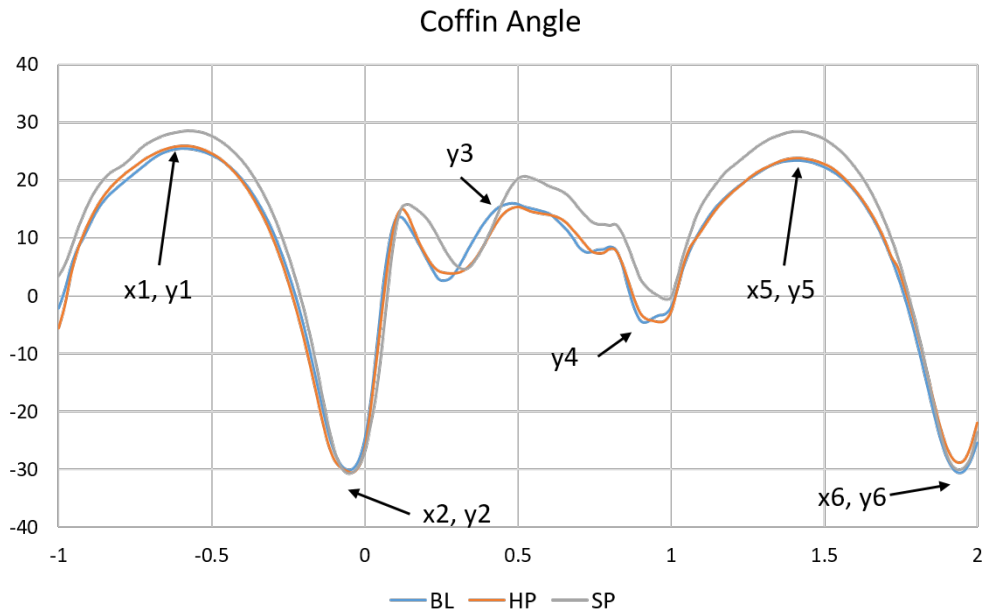

Coffin joint excursion at trot. Average for five horses on baseline (BL), hard perturbation (HP) and soft perturbation (SP)

The hard perturbation at trot (Table, column 3) had a significant effect on the maximal coffin flexion during the swing phase (y3) and on the maximal coffin extension at the end of the second stance phase (y6). The hard perturbation decreased the amplitudes of both the maximal flexion during the swing phase and the extension peak at the end of the second stance phase.

The soft perturbation at trot (Table, column 4) had a significant effect on the coffin flexion peak of the first stance phase (y1), on the maximal flexion of the swing phase (y3), and on the flexion peak of the second stance phase (y5). It also had a non-significant effect on the maximal extension during the swing phase. The soft perturbation increased the flexion peaks of both stance phases and the maximal flexion and extension of the swing phase, and slightly delayed the flexion peak of the second stance phase.

Trotting velocity (Table, column 5) had a significant effect on the flexion peaks of both stance phases (y1, y5), on the extension peak of the first stance phase (y2) and on the maximal flexion during the swing phase (y3). With increasing velocity, the flexion amplitudes of both stance phases and the maximal flexion of the swing phase increased, and the extension peak of the first stance phase decreased.

Table: Effects of perturbation and velocity on the coffin joint excursion at trot, coefficient, (p-value), and r^2 (* P<0.05)

	Intercept	HardPert	SoftPert	Velocity	r2
x1	-0.59* (0.0000)	0.00 (0.8465)	0.01 (0.1927)	-0.00 (0.8370)	0.63
y1	-5.70 (0.4398)	0.15 (0.8291)	2.24* (0.0029)	9.73* (0.0000)	0.93
x2	-0.09 (0.0759)	-0.00 (0.5052)	-0.00 (0.9570)	0.01 (0.4463)	0.14
y2	-47.80* (0.0000)	-0.60 (0.4345)	-0.81 (0.3244)	5.27* (0.0130)	0.96
y3	-0.93 (0.9343)	-3.36* (0.0049)	3.74* (0.0033)	7.38* (0.0214)	0.87
y4	-33.70* (0.0057)	-0.93 (0.4105)	-2.21 (0.0696)	2.57 (0.4030)	0.92
x5	1.47* (0.0000)	0.00 (0.7939)	0.02* (0.0306)	-0.02 (0.4262)	0.29
y5	2.69 (0.7847)	0.21 (0.8381)	4.60* (0.0001)	6.51* (0.0232)	0.83
x6	2.04* (0.0000)	-0.01 (0.1884)	0.01 (0.3091)	-0.03 (0.1901)	0.25
y6	-43.77* (0.0000)	3.23* (0.0003)	1.36 (0.1339)	3.57 (0.1241)	0.95

Representative data are presented for strain calculated in the Straight Sesamoidean Ligament under the three conditions, at trot.

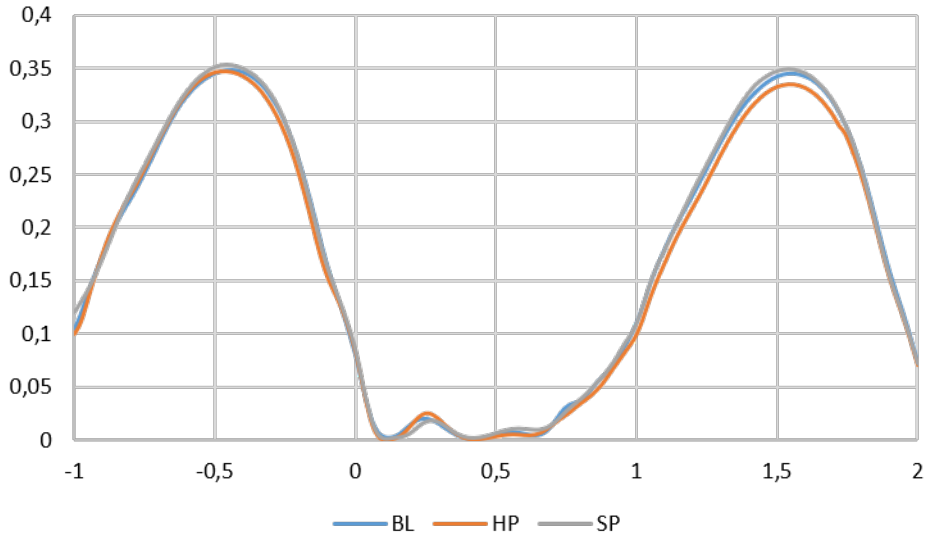

Figure: Straight Sesamoidean Ligament strain at trot. Average for five horses on baseline (BL), hard perturbation (HP) and soft perturbation (SP)

Table: Effects of perturbation and velocity on the Straight Sesamoidean Ligament strains and strain rates at trot, coefficient, (p-value), and r^2 (* P< 0.05) (St1 is first stance phase and St2 is second stance phase)

	Intercept	HardPert	SoftPert	Velocity	r2
MaxStrainSt1	0.273* (0.0000)	-0.003 (0.1672)	0.003 (0.1524)	0.024* (0.0001)	0.97
MaxStrainSt2	0.261* (0.0000)	-0.012* (0.0000)	0.001 (0.6930)	0.027* (0.0001)	0.95
MaxStrainRateSt1	0.024 (0.9853)	0.807* (0.0000)	-0.086 (0.5788)	0.889* (0.0257)	0.74
MaxStrainRateSt2	1.103 (0.4497)	-0.122 (0.4475)	0.209 (0.2242)	0.549 (0.2086)	0.71

The hard perturbation at trot (Table, column 3) had a significant effect on the maximal strain of the SSL during the second stance phase and on the maximal strain rate during the first stance phase. With the hard perturbation, the SSL was less strained during the second stance phase, and the strain rate

during the first stance phase was greater. The soft perturbation at trot (Table, column 4) did not have a significant effect on the maximal strains and strain rates of the SSL.

Conclusion

The two main objectives of this study were (1) to determine when and how the limb responds when hitting an unexpectedly harder or softer surface and (2) to study if this response can be quantified using a musculoskeletal model, through alterations in joint motions and calculated tendon and ligament strains.

(1) The data indicate that the horse did respond to the perturbation of its gait. In response to the soft perturbation, the proximal limb stiffened during the perturbed stance phase, but was then unchanged from the baseline in the second stance phase. The increased amplitude of movement observed in the distal joints was likely a consequence of the alterations of the proximal joints. In response to the hard perturbation, the proximal limb was more flexed during the swing phase and the second stance phase, but was unchanged from the baseline in the perturbed (first) stance phase. The distal limb at trot was largely unaffected by the hard perturbation with the exception of increased hyperextension of the carpus in the perturbed stance phase and less fetlock hyperextension in the second stance phase. At canter, the distal limb responded to the hard perturbation with reduced fetlock hyperextension in the perturbed stance phase, and otherwise all three distal joints were more flexed in the swing phase.

(2) Although the musculoskeletal model developed was a preliminary model with some deficiencies noted in the muscle models in particular, it was possible to observe the reaction of the forelimb to the perturbation. The alterations observed in joint motions led to changes in ligament and tendon strains. In response to the soft perturbation, the alterations in shoulder and elbow angles resulted in increased strain in the lacertus fibrosus at the stance-swing phase transition, and the increased coffin flexion in both stance phases resulted in increased strain in the radial and ulnar tendons of the deep digital flexor and in the suspensory ligament's extensor branches. In response to the hard perturbation, the alterations in shoulder and elbow angles resulted in increased strain in the lacertus fibrosus at the stance-swing phase transition.

The horse forelimb responded differently to the hard and to the soft perturbations. The ground hardness of the perturbations was not quantified, but it was subjectively observed that the soft perturbation seemed to introduce a more observable behavioural change than the hard perturbation. The differences in reaction to the perturbations might be a consequence of the severity of the hardness change and not of its nature (softer vs harder). It could be supposed that the differences in response delay was a consequence of the difference of the severity of the hardness change whereas

the stiffening/softening response of the proximal limb can be thought to be due to the nature of the hardness change.

To discriminate the effect of the severity of the perturbation, it would be necessary to collect data with at least two different levels of intensity for each type of perturbation (soft and hard), and if possible, with similar magnitude of hardness change for both soft and hard perturbations.

Further development of the model with refinement of the muscle models will enable better assessment of individual muscles in the limb, and their contributions to development of force in tendons crossing joints. These contributory forces will have consequent effects on strains calculated for the passive ligaments in the model.